Contour-based models for 3D binary reconstruction in X-ray tomography

C. Soussen* and A. Mohammad-Djafari*

*Laboratoire des Signaux et Systèmes
Supélec, Plateau de Moulon, 91192 Gif–sur–Yvette Cedex, France

Abstract. We study the reconstruction of a 3D compact homogeneous object lying inside a homogeneous background for computer aided design (CAD) or nondestructive testing (NDT) applications. Such a binary scene describes either a solid object or an homogeneous material in which a fault is sought. The goal in both cases is to reconstruct the shape of the scene from sparse radiographic data. This problem is under-determined and one needs to use all prior information about the scene to find a satisfactory solution. A natural approach is to model the exterior contour of the fault by a deformable *geometric template*, which we reconstruct directly from the radiographic data. In this communication, we give a synthetic view of these contour-based methods and compare their relative performances and limitations to recover complex faults.

INTRODUCTION

In computer aided design (CAD) or nondestructive testing (NDT) of materials, one traditionally retrieves 3D scenes from shadows or X-ray tomographic data. In CAD, these scenes describe solid materials for which we seek a computer description of the surface. In NDT, they correspond to homogeneous materials in which some faults are sought.

In the case where a compact fault $\mathcal{C}$ is already detected and its shape is to be reconstructed, the scene $\mathcal{S}$ is composed of two regions of constant density, for example 1 and 0; then, the density function of the scene is written

$$f(x) \;=\; \begin{cases} 1 & \text{if } x \text{ is inside the fault } \mathcal{C}, \\ 0 & \text{otherwise.} \end{cases} \tag{1}$$

The reconstruction problem is under-determined due to sparsity of the data: both number and angles of projections are limited. One then needs to use all prior information about the fault and the background to find a satisfactory solution.

A first approach is to use the binary characteristics of the voxels of the scene and a Markov random field (MRF) to model the homogeneity of both materials [1]. A more natural approach is to model the exterior contour of $\mathcal{C}$ (that we also denote $\mathcal{C}$ for sake of simplicity) by a deformable *geometric template*, which we reconstruct directly from the radiographic data [2, 3, 4, 5, 6, 7]. Among geometric models, we study explicit parametric descriptions. Possible models are quadrics, superquadrics, harmonic surfaces, and splines.

The first three categories of models are global but the last is *local* in its parameters. In particular, we discuss first order spline models which yield polyhedral shapes [3, 8, 7]. In recent works [9, 7], we have proposed regularization-based methods to estimate the vertices coordinates of a polyhedron directly from the projections. In this communication, we give a synthetic view of these contour-based methods and compare their relative performances and limitations to recover complex faults.

Direct problem and scene modeling

We model the data vector $\boldsymbol{d}$ as the noisy line projections of the density function:

$$\boldsymbol{d} \;=\; \mathcal{A}(\mathcal{S}) + \boldsymbol{n}, \tag{2}$$

where $\mathcal{A}$ is the projection operator and $\boldsymbol{n}$ is the noise process, which we assume additive, *i.i.d.* and Gaussian for the sake of simplicity. In other words, we model each piece of data as the integral of the density function $f(x)$ along the line arriving at the center of the corresponding detector pixel. There exist more accurate (and complex) models which account for the whole area of the detector pixels. Projections are then based on strip band integration of $f(x)$, see [10] for example.

Assume we model the scene $\mathcal{S}$ by a set of n binary cubic voxels $\boldsymbol{f} = [f_1, \ldots, f_n]^t$, where each voxel value is equal to 1 if the centre of the voxel is inside the fault, and 0 otherwise [11, 1]. Operator $\mathcal{A}$ becomes linear towards $\boldsymbol{f}$ and equation (2) rereads

$$\boldsymbol{d} \;=\; \boldsymbol{A}\boldsymbol{f} + \boldsymbol{n}, \tag{3}$$

where $\boldsymbol{A}$ stands for the X-ray projection matrix, whose elements are the length of the intersections between each voxel and each projection line.

In case of contour reconstruction, the scene is described by the contour $\mathcal{C}$ of the fault region. Assuming the whole background area has a null density, it has no contribution on the scene projection. Then, we rewrite the projection operator $\mathcal{A}(\mathcal{C})$. The main difference from voxel representation is that the projection operator is nonlinear with respect to contour parameters, and this leads to complex optimization problems. However, the number of those parameters is significantly smaller than the dimension of a voxel representation $\boldsymbol{f}$.

Bayesian estimation

We use Bayesian methodology to perform the reconstruction. It affords the definition of a posterior density of probability $p(\mathcal{S}|\boldsymbol{d})$ by accounting for the noise process and a prior $p(\mathcal{S})$ on the scene, which models our physical knowledge of both fault and background. Bayes rule leads to the expression of $p(\mathcal{S}|\boldsymbol{d})$:

$$p(\mathcal{S}|\boldsymbol{d}) \;=\; \frac{p(\boldsymbol{d}|\mathcal{S})\, p(\mathcal{S})}{p(\boldsymbol{d})}, \tag{4}$$

where $p(\boldsymbol{d})$ is a normalization factor. We select the *maximum a posteriori* (MAP) estimator $\widehat{\mathcal{S}}$, *i.e.,* the scene which maximizes the posterior law. Then, it also minimizes the negative of its logarithm.

$$\widehat{\mathcal{S}} \;=\; \arg\min_{\mathcal{S}} \{-\log p(\mathcal{S}|\boldsymbol{d})\} \;=\; \arg\min_{\mathcal{S}} \{-\log[p(\boldsymbol{d}|\mathcal{S})\, p(\mathcal{S})]\}. \tag{5}$$

Denoting by σ^2 the variance of the noise process $\boldsymbol{n}$, $\widehat{\mathcal{S}}$ minimizes the functional

$$\mathcal{J}(\mathcal{S}) \;=\; \| \boldsymbol{d} - \mathcal{A}(\mathcal{S}) \|^2 \,-\, (2\pi\sigma^2)^M \,\log p(\mathcal{S}), \tag{6}$$

where M is the number of data. Criterion $\mathcal{J}$ is then defined as the sum of two terms, a fidelity to data term that we denote $\mathcal{K}(\mathcal{S}) = \| \boldsymbol{d} - \mathcal{A}(\mathcal{S}) \|^2$, and a regularization term, which corresponds to the prior information. In fact, we define $-\log p(\mathcal{S}) \propto \mathcal{R}(\mathcal{S}) + K$, where K is a constant term, and functional $\mathcal{J}$ is then equal to

$$\mathcal{J}(\mathcal{S}) \;=\; \mathcal{K}(\mathcal{S}) + \lambda \mathcal{R}(\mathcal{S}), \tag{7}$$

up to a constant term. In the next sections, we specify $\mathcal{R}(\mathcal{S})$ for each scene model.

VOXEL BASED RECONSTRUCTION

If we define the 3D scene by a set of n binary cubic voxels $\mathcal{S} \equiv \boldsymbol{f} = [f_1, \ldots, f_n]^t$, the main prior knowledge is that image $\mathcal{S}$ is piecewise homogeneous. That leads to the definition of a Markov random field, with the following energy:

$$\mathcal{J}(\boldsymbol{f}) \;=\; \mathcal{K}(\boldsymbol{f}) + \lambda \sum_{i \sim j} \varphi(f_i - f_j), \tag{8}$$

where $\mathcal{K}(\boldsymbol{f}) = \|\boldsymbol{d} - \boldsymbol{A}\boldsymbol{f}\|^2$, φ is an even function, nondecreasing on $\mathbf{R}^+$, and "$\sim$" denotes the neighborhood relation between voxels [1]. Minimization of $\mathcal{J}$ is not straightforward since it has to be done over the discrete set $\{0,1\}^n$. We choose to extend and optimize $\mathcal{J}$ on a continuous domain, *i.e.,* $\mathcal{X} = (0,1)^n$ for algorithmic purposes. Function φ is chosen to be convex, we practically use the Huber function, which is quadratic towards 0 and linear at infinity [12]. Functional $\mathcal{J}$ is then convex as a sum of two convex functions. Then, minimization of $\mathcal{J}$ over $\mathcal{X}$ can be carried out by gradient-based techniques.

The above modeling does not account for our other physical knowledge, *i.e.,* the density values of each material. Following the work of Gautier [13], we add a second regularization term which biases the value of all voxels to the metal, *i.e.,* 0. The posterior density finally writes:

$$\mathcal{J}(\boldsymbol{f}) \;=\; \mathcal{K}(\boldsymbol{f}) + \lambda \sum_{i \sim j} \varphi(f_i - f_j) + \mu \sum_i |f_i|^\alpha, \tag{9}$$

where $1 < \alpha < 2$. As in the case where $\mu = 0$, $\mathcal{J}$ is convex and differentiable, then gradient-based methods can be used to obtain the MAP estimate.

However, this modeling does not account for fault compacity. Moreover, the size of $\boldsymbol{f}$ is huge for a high resolution sampling of the scene, and voxel reconstruction may be computationally expensive. For these reasons, we study direct compact shape reconstruction procedures.

CONTOUR BASED RECONSTRUCTION

We here directly take advantage of the binary compact nature of the object. Instead of reconstructing the volume of $\mathcal{S}$, we choose to model the contour $\mathcal{C}$ by a deformable template and estimate its parameters from the radiographic data. There are several ways of modeling geometric templates.

The first is to define implicitly the contour $\mathcal{C}$ as the zero-th level-set of a function $\Phi : \mathbf{R}^3 \longrightarrow \mathbf{R}$ [5, 6].

$$\mathcal{C} \;=\; \{x \in \mathbf{R}^3 : \Phi(x) = 0\}. \tag{10}$$

The principle of level-set methods is to define an evolution law for Φ ($\Phi(x,t)$ now depends on a time parameter t) and to update its level-set $\mathcal{C}_t$. This approach needs a transformation of the implicit curve $\mathcal{C}_t$ into voxels in order to calculate approximate projections of scenes $\mathcal{S}_t$. Such projection processes yield time consuming reconstruction algorithms.

In the following, we only consider "fully geometric" models, *i.e.,* parametric contours. We define a set of parameters $\boldsymbol{a}$ and the corresponding contour $\mathcal{C}_{\boldsymbol{a}}$. Estimation of $\widehat{\boldsymbol{a}}$ is done by least-square (LS) or MAP techniques.

$$\widehat{\boldsymbol{a}} = \arg\min_{\boldsymbol{a}} \{\mathcal{J}(\boldsymbol{a}) = \mathcal{K}(\boldsymbol{a}) + \lambda \mathcal{R}(\boldsymbol{a})\}, \text{ with } \mathcal{K}(\boldsymbol{a}) = \|\boldsymbol{d} - \mathcal{A}(\mathcal{C}_{\boldsymbol{a}})\|^2, \tag{11}$$

where, as in section , $\mathcal{K}(\boldsymbol{a})$ accounts for fidelity to data and $\mathcal{R}(\boldsymbol{a})$ is a regularization term. LS estimation corresponds to $\lambda = 0$. We distinguish two types of parameterized surfaces: *local* and *global* ones. A surface is said local with respect to its parameters $\boldsymbol{a}$ if for each parameter a_i, a modification of a_i yields a move of only part of the surface $\mathcal{C}_{\boldsymbol{a}}$. One obviously needs a local parameterization to describe arbitrary nonconvex and irregular contours. However, in the following, we also consider global parameterization of contours by a limited number of parameters since it can retrieve the low frequency features of contours.

In any case, the difficulty is the calculation of $\mathcal{K}(\boldsymbol{a})$, in fact the evaluation of the projections $\mathcal{A}(\mathcal{C}_{\boldsymbol{a}})$. For specific models, analytic expressions of $\mathcal{A}(\mathcal{C}_{\boldsymbol{a}})$ are not available, we then use a polyhedral approximation $\mathcal{P}_{\boldsymbol{a}}$ of $\mathcal{C}_{\boldsymbol{a}}$, whose computation of projections may be expensive depending on the number of vertices of $\mathcal{P}_{\boldsymbol{a}}$.

The rest of the section is organized as follows: we first consider very simple global models, then define more complex ones, leading to star-shaped contours. Finally, we study the case of splines and their ability to reconstruct various shapes.

Quadrics and Superquadrics

Quadrics/Superquadrics are very simple shapes since they only depend on few parameters. Superquadrics are generalizations of quadrics and yield *nonconvex* and *star-shaped* shapes. These contours have mainly been used in image segmentation [14]. Considering a super-ellipsoid as a star-shaped contour, and denoting $\boldsymbol{G}$ its central point, this

surface is defined by:

$$\boldsymbol{GM}(\theta,\phi) \;=\; [a\sin^{\alpha}\phi\cos^{\beta}\theta,\, b\sin^{\alpha}\phi\sin^{\beta}\theta,\, c\cos^{\alpha}\phi]^t, \tag{12}$$

where $\theta \in (0, 2\pi)$, $\phi \in (0, \pi)$, and α, β are positive parameters. Definition (12) is based on spherical coordinates as illustrated on figure 1. Surface parameters are $\{\boldsymbol{G}, a, b, c, \alpha, \beta\}$. Quadrics correspond to $\alpha = \beta = 1$.

Practically, we first estimate the position $\boldsymbol{G}$ and the axes of inertia of $\mathcal{C}$ from the data using explicit relations between the moments of the projections and those of the object [3, 15]. Then, we process the development (12) in the basis formed by these axes, where the third coordinate corresponds to the greatest moment of inertia. Estimation of $\boldsymbol{a} = [a, b, c, \alpha, \beta]^t$ is done by a constrained least-square method (*i.e.,* $\lambda = 0$ in equation (11)) and a gradient based algorithm whose initialization corresponds to a sphere. We set the constraints $0 < a < b < c$ and $0.2 < \alpha, \beta < 3$; the latter avoids degenerate shapes.

Harmonic contours

We consider the following generalization of superquadrics. Surface harmonics are star shaped surfaces defined on the unit sphere of $\mathbf{R}^3$ (see [16, 17] for their use in image segmentation). Using notations of figure 1, we define the general parameterization:

$$\boldsymbol{GM}(\theta,\phi) \;=\; \rho(\theta,\phi)\,[\sin\phi\cos\theta, \sin\phi\sin\theta, \cos\phi]^t. \tag{13}$$

We now use the following property [16]. Any function $\rho(\theta, \phi)$ of finite energy and differentiable on the unit sphere of $\mathbf{R}^3$ can be decomposed as a linear combination of spherical harmonics:

$$\rho(\theta,\phi) \;=\; \sum_{l=0}^{\infty} \sum_{|m|\le l} a_l^m\, \rho_l^m(\theta,\phi), \tag{14}$$

where spherical harmonics ρ_l^m are linked to Legendre polynomials [16]. Introducing a cut off L, we consider the family $\mathcal{H}_L$ of surface harmonics whose coefficients a_l^m are null for $l > L$. The vector parameter is then $\boldsymbol{a} = \{a_l^m, |m| \le l \le L\}$. The star shaped constraint reads

$$\rho(\theta,\phi) > 0, \;\; \forall(\theta,\phi), \tag{15}$$

leading to *unintersected* surfaces. As for superquadrics, parameterization (13) is done with respect to the basis formed of the estimated inertia axes of $\mathcal{C}$. Projection of surfaces of $\mathcal{H}_L$ are evaluated by their sampling into polyhedra $\{\boldsymbol{M}_{i,j} = \boldsymbol{M}(\theta_{i,j}, \phi_{i,j})\}$. Estimation of $\boldsymbol{a}$ is done by a constrained least-square technique. Constraints are $\rho_{i,j} > \varepsilon$ for all i and j, where ε is an arbitrary threshold.

Splines

A common and convenient way to describe local shapes is spline modeling; see [18, 19] for 2D spline curves reconstruction and [20] for 3D spline curves reconstruction in

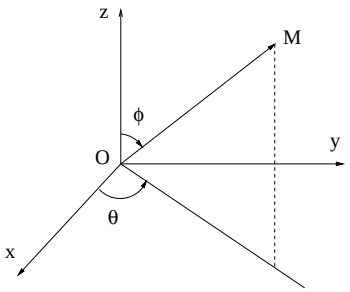

FIGURE 1. Spherical coordinates.

tomography. Parameters $\boldsymbol{a}$ are the control points $\{\boldsymbol{a}_i, i = 1, \ldots, n\}$ of the spline model. This model is local since each point $\boldsymbol{a}_i$ affects only a part of $\mathcal{C}_{\boldsymbol{a}}$. More precisely, spline representation is based on the arc length of the contour. For example, in 2D case, spline modeling reads as follows.

$$(x(s), y(s))^t \quad = \quad \sum_{i=1}^{n} B_i(s)\, \boldsymbol{a}_i, \tag{16}$$

where functionals $B_i(s)$ are B-spline basis functions of bounded support, and extremal points $\boldsymbol{a}_n$ and $\boldsymbol{a}_1$ are equal, to generate a closed surface. The choice of the order of the spline, *i.e.*, of polynomials B_i is not straightforward. A large order yields smooth contours and a larger degree of locality, whereas a small order does not favor global smoothness. In the following, we choose first-order splines, *i.e.*, polygons and polyhedra; in other words, functions B_i are affine on their corresponding arc length interval, and $\mathcal{C}_{\boldsymbol{a}}(s)$ is piecewise affine. The reasons for that choice are mostly algorithmic. Indeed, computation of projections of first-order splines is fairly straightforward since it only requires intersections of projection rays and object edges (faces) of the polygon (polyhedron). Cunningham *et al.* [18, 8, 4] have derived similar models but the method they use for computation of projections is not direct. It is an approximate evaluation based on a transformation of the scene into a set of voxels and the use of classical voxel set projections routines. However, that method is more easily extendable to strip band integration [4]. Both strategies are illustrated on figure 2. The direct projection evaluation is still simple in 3D case provided the polyhedral faces are triangular. In the following, we first develop the 2D method, and then its extension to 3D case.

Polygonal shapes

A polygon $\mathcal{P}$ is defined as a closed connection of vertices: $\mathcal{P}_{\boldsymbol{a}} \equiv \{\boldsymbol{a}_1, \ldots, \boldsymbol{a}_n\}$, $\boldsymbol{a}_i \in \mathbb{C}$, where vertices $\boldsymbol{a}_i$ are arranged in the anti-clockwise order. Hence, fault reconstruction is equivalent to estimation of positions $\boldsymbol{a}_i$ subject to the following constraint: the edges of $\mathcal{P}$ do not intersect. In recent years, we have developed a regularization method to reconstruct polygonal shapes from sparse tomographic data [21, 9]. With notations of equation (11), we estimate a MAP solution $\widehat{\boldsymbol{a}}$ by minimizing the *a posteriori* energy $\mathcal{J}(\boldsymbol{a})$, where the regularization functional tends to favor local smoothness of $\mathcal{P}_{\boldsymbol{a}}$. We

then use Markovian based penalizations [9]:

$$\mathcal{R}(\boldsymbol{a}) \;=\; \sum_{j=1}^{n} \phi(|\boldsymbol{a}_i - (\boldsymbol{a}_{i-1} + \boldsymbol{a}_{i+1})/2|), \tag{17}$$

where ϕ is a nondecreasing function. Algorithmic aspects are similar to the 3D case and will be discussed in the next paragraph.

Polyhedral shapes

Recently, several researchers have developed 3D polyhedral reconstruction methods [22, 8, 7]. Generalizing the 2D modeling, we define a closed polyhedron $\mathcal{P}_{\boldsymbol{a}} = (\boldsymbol{a}, \mathcal{F})$ by a set of n vertices $\boldsymbol{a} = \{\boldsymbol{a}_1, \ldots, \boldsymbol{a}_n\} \in \mathbf{R}^{3n}$ and a set of triangular faces $\mathcal{F}$. For a fixed n and fixed faces, the *a posteriori* energy $\mathcal{J}(\boldsymbol{a})$ defined in (11) depends on $\boldsymbol{a}$ only. The MAP estimate is then

$$\widehat{\boldsymbol{a}} \;=\; \arg\min_{\boldsymbol{a}} \mathcal{J}(\boldsymbol{a}). \tag{18}$$

Following (17), regularization $\mathcal{R}(\boldsymbol{a})$ tends to enforce the local regularity of $\mathcal{P}$. We consider Euclidean distances between each vertex $\boldsymbol{a}_i$ and the center of gravity $\boldsymbol{a}_i^\star$ of its neighbors.

$$\mathcal{R}(\boldsymbol{a}) \;=\; \sum_{i=1}^{n} \phi(\|\boldsymbol{a}_i - \boldsymbol{a}_i^\star\|), \tag{19}$$

where ϕ is a nondecreasing function. We select a nonconvex function, such as the truncated quadric. Such a function penalizes equally any distance $\|\boldsymbol{a}_i - \boldsymbol{a}_i^\star\|$ greater than some arbitrary threshold, and then allows large deformations of vertices. Other choices are available for $\mathcal{R}$; see [4] for curvature based regularizations.

In the above formulation, the projection operator $\mathcal{A}$ is highly nonlinear as a function of the coordinates of $\boldsymbol{a}_i$. That generally leads to multimodal criteria $\mathcal{K}$ and $\mathcal{J} = \mathcal{K} + \lambda\mathcal{R}$. Practical difficulties are then related to the global optimization of $\mathcal{J}$. We use *local* techniques (gradient descent or relaxation procedures), which provide a local minimizer of $\mathcal{J}$. As in the case of harmonic models, the key point is to select an initial solution close enough to the global minimizer of $\mathcal{J}$. In practice we use the harmonic modeling method described in section both to select n[1] and as an initial guess to the polyhedral method.

---

[1] Selection of n depends on the cut off parameter L that defines the harmonic contour. The greater L, the higher the spatial frequencies contained in the contour; a high value of L then leads to an increase of n to produce an accurate polyhedral approximation of the harmonic shape.

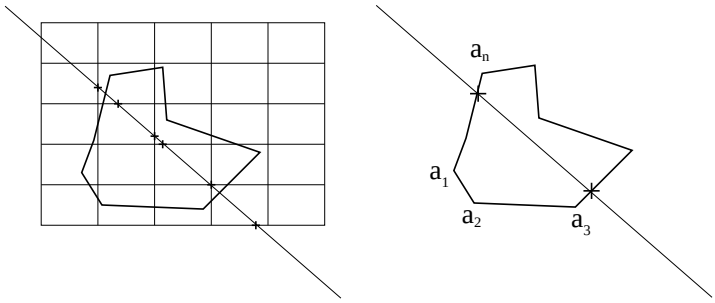

FIGURE 2. Projection calculation in 2D case. a) Approximate numerical computation, based on discretization of $\mathcal{C}$ into pixels. Calculation is then done using the linear operator $\boldsymbol{A}\boldsymbol{f}$ introduced in section . Here, vector $\boldsymbol{f}$ is not forcibly binary, the value of each pixel (i) crossing an edge of $\mathcal{C}$ is the proportion of the surface of $\mathcal{C} \cap (i)$ over the surface of (i). b) Exact *analytic* calculation, based on the positions of the intersections between projection rays and polyhedron edges.

SIMULATION RESULTS

The main objective of these simulations is to point out the advantages and limitations of each contour based approach. To this end, we present the reconstructions obtained on a common data set. Data are 9 noisy parallel projections of a synthetic object $\mathcal{C}$. All projections correspond to a common detector, set on a plane $z = constant$ (see figure 3 for the illustration of the object, the projection geometry, and the data). The signal to noise ratio (SNR) is 10 dB and the resolution of each set of projection data is 64×64 pixels. Apart from the limited number and angles of the projections, the difficulty lies in the fact that the object shape is highly nonconvex.

As represented on the first graph of figure 4, the ellipsoidal reconstruction obtained by the moment based technique [15] is clearly poor since it does not provide information on the “foot" of the mushroom. Moreover, estimation of the main axis of inertia of $\mathcal{C}$ is incorrect. On the second graph of this figure, we represent the superquadric estimated from the data by the constrained LS method presented in section . This result does not clearly enhance the quality of reconstruction. In fact, the variety of superquadrics is not wide enough to describe a complex object, even though this family may yield nonconvex shapes.

In figure 5, we represent the harmonic contour reconstructions for different numbers of parameters a_l^m (7 and 14). Harmonic development is done relatively to the axes of inertia obtained by the moment based technique (see the orientation of the ellipsoid of figure 4 (a)). Reconstructed shapes are nonconvex and closer to the real object, although the second one has a relatively high computational cost (150 seconds CPU). In fact, harmonic modeling may not produce high resolution results unless the order L of the development (14) is huge. In that case, discretization of the contour needs to be fine and then, both projection calculation and reconstruction process are a computational burden.

Finally, we show the results of the polyhedral method with the above mentioned reconstructions as initializations (see figure 6). The local optimization technique is a gradient descent algorithm. The first two results correspond to ellipsoidal and super-

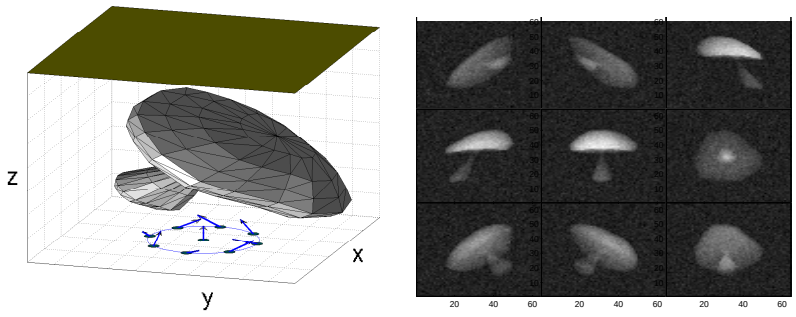

a) b)

FIGURE 3. a) Original object and projection geometry, b) Simulated data, composed of 9 noisy projection images of 64×64 pixels. SNR of the data is 10 dB.

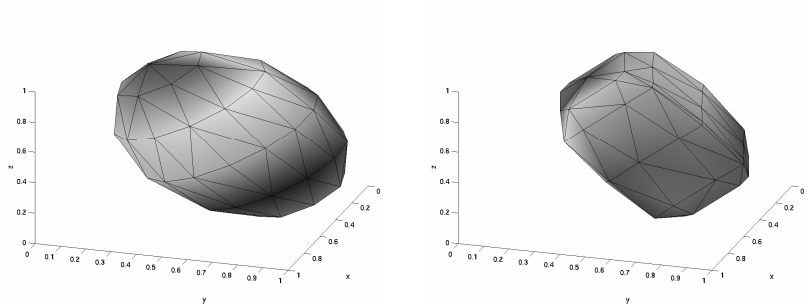

a) b)

FIGURE 4. Ellipsoid and super-ellipsoid reconstructed from the data. a) Ellipsoid reconstruction by the moment based method, b) Superquadric reconstruction by the constrained least-square method, using the center and axes of inertia of a).

ellipsoidal initializations. They only contain the low frequency features of the mushroom since initializations are too distant from the real object. Results obtained with harmonic initializations are clearly more accurate (see the second line of figure 6). The quality of the final reconstruction is then highly related to the initialization, although a complex initialization yields an increase of the number n of vertices. In addition to those results, computational cost of the polyhedral method is 150 and 186 seconds CPU for cases a) and b), which is relatively low compared to the one of voxel methods.

CONCLUSION

In this paper, we have presented several methods of reconstruction of compact faults from sparse X-ray tomographic data. These methods are all based on an explicit parametric modeling of the external shape of the homogeneous object and the direct estimation of those parameters from the data. In contrast to global modelings, the polyhedral approach affords high quality reconstructions of nonconvex objects in a limited computational time. However, reconstructions are highly dependent on the initialization since

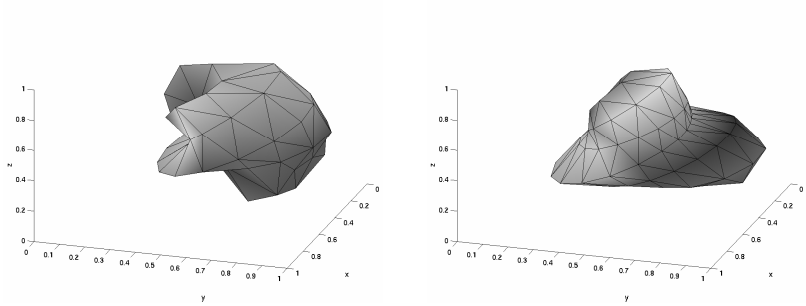

a) b)

FIGURE 5. Surface harmonic reconstructions. a) Choice of 7 parameters, discretization of the surface into a polyhedron of 58 vertices and 95 triangles, b) Choice of 14 parameters, discretization into a polyhedron of 112 vertices and 186 triangles.

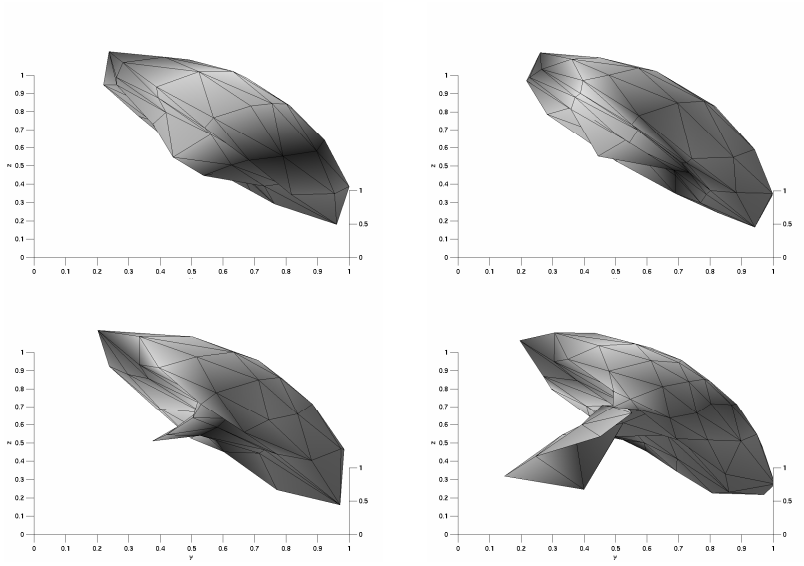

FIGURE 6. Polyhedral reconstructions with various initializations, which are the results of quadric, superquadric, or harmonic methods. First row: initialization by the ellipsoid and super-ellipsoid represented on figure 4. Second row: initialization by the harmonic surfaces represented on figure 5. Visualization is done up to a rotation to have a better view of the “foot" of the mushroom.

the energy to be minimized is generally multimodal. We then recommend the combination of the three methods:

1. Using the moment based method to estimate the center of gravity of the object and the position of its axes of inertia.
2. Using the surface harmonic modeling to obtain an accurate initialization.
3. Using spline modeling to perform final reconstruction.

Future works will involve multiresolution procedures [18, 23] that may help to obtain a better initialization. We also plan to evaluate geometric methods on real data and to study their extension to the case where interior and exterior densities of the object are

still uniform, but unknown. One then needs to estimate those parameters in addition to the contour shape.

REFERENCES

1. K. D. Sauer, J. J. Sachs, and C. Klifa, "Bayesian estimation of 3-D objects from few radiographs," *IEEE Trans. Nuclear Sciences*, **41**, pp. 1780–1790, October 1994.
2. K. M. Hanson, "Bayesian reconstruction based on flexible prior models," *J. Opt. Soc. Amer.*, **10**, pp. 997–1004, May 1993.
3. P. Milanfar, W. C. Karl, and A. S. Willsky, "Reconstructing binary polygonal objects from projections: A statistical view," *Computer Vision and Graphics and Image Processing*, **56**, pp. 371–391, September 1994.
4. X. L. Battle, G. S. Cunningham, and K. M. Hanson, "Tomographic reconstruction using 3D deformable models," *Phys. Med. Biol.*, **43**, pp. 983–990, 1998.
5. S. Teboul, L. Blanc-Féraud, G. Aubert, M. Barlaud, and J. Darcourt, "Contours déformables et reconstruction tomographique en imagerie médicale," in *Actes du 16*e *colloque GRETSI*, (Grenoble, France), pp. 1495–1498, September 1997.
6. R. T. Whitaker, "A level-set approach to 3D reconstruction from range data," *Int. J. Computer Vision*, **29**, (3), pp. 203–231, 1998.
7. C. Soussen and A. Mohammad-Djafari, "Multiresolution approach to the estimation of the shape of a 3D compact object from its radiographic data," in *Proc. SPIE, Mathematical Modeling, Bayesian Estimation, and Inverse Problems*, F. Prêteux, A. Mohammad-Djafari, and E. R. Dougherty, eds., (Denver, CO, USA), pp. 150–160, July 1999.
8. X. L. Battle, G. S. Cunningham, and K. M. Hanson, "3D reconstruction using geometrical models," in *Proc. SPIE*, vol. 3034, (San Diego, CA, USA), pp. 346–357, 1997.
9. A. Mohammad-Djafari and C. Soussen, "Compact object reconstruction," in *Discrete Tomography: Foundations, Algorithms and Applications*, G. T. Herman and A. Kuba, eds., ch. 14, pp. 317–342, Birkhauser, Boston, 1999.
10. A. C. Kak and M. Slaney, *Principles of Computerized Tomographic Imaging*, IEEE Press, New York, 1988.
11. J.-M. Dinten, "Tomographic reconstruction of axially symmetric objects: Regularization by a Markovian modelisation," in *Proc. of the Int. Conf. on Pattern Recog.*, 1990.
12. P. J. Huber, *Robust Statistics*, Wiley, John, New York, 1981.
13. S. Gautier, *Fusion de données gammagraphiques et ultrasonores. Application au contrôle non destructif*. PhD thesis, Université de Paris-Sud, Orsay, December 1996.
14. F. Solina and R. K. Bajcsy, "Recovery of parametric models from range images: The case for superquadrics with global deformations," *IEEE Trans. Pattern Anal. Mach. Intell.*, **PAMI-12**, pp. 131–147, February 1990.
15. C. Soussen and A. Mohammad-Djafari, "Recovery of moments of a compact homogeneous object from tomographic projection data," Technical Report submitted to *Graphical Models and Image Processing*, GPI–LSS, 1999.
16. A. Matheny and D. B. Goldgof, "The use of three and four-dimensional surface harmonics for rigid and nonrigid shape recovery and representation," *IEEE Trans. Pattern Anal. Mach. Intell.*, **17**, pp. 967–981, October 1995.
17. G. Lefaix, X. Riot, P. Haigron, R. Collorec, and A. Ramee, "3D modeling and deformation analysis of the vertebra with spherical harmonics," in *Proceedings of the 19th Annual International Conference of the IEEE Engineering in Medicine and Biology Society*, vol. 1, (Chicago, IL, USA), pp. 422–425, November 1997.
18. G. S. Cunningham, I. Koyfman, and K. M. Hanson, "Improved convergence of gradient-based reconstructions using multi-scale models," *Medical Imaging: Image Processing, Proc. SPIE*, **2710**, pp. 145–155, 1996.
19. F. Coutand, L. Garnero, and J. Fonroget, "Anatomical data fusion for quantitative reconstruction in myocardial tomoscintigraphy using a spline model of the thorax organs," *IEEE Trans. Biomedical Engineering*, **44**, pp. 575–584, July 1997.

20. B. Chalmond, F. Coldefy, and B. Lavayssière, “3D curve reconstruction from noisy projections,” in *Wavelets, Images and Surface Fitting*, P.-J. Laurent, A. Le Méhauté, and L. L. Schumaker, eds., pp. 113–119, Peters, A. K., 1994.
21. A. Mohammad-Djafari, “Binary polygonal shape image reconstruction from a small number of projections,” *Elektrik*, **5**, (1), pp. 127–138, 1997.
22. P. Milanfar, W. C. Karl, and A. S. Willsky, “A moment-based variational approach to tomographic reconstruction,” *IEEE Trans. Image Processing*, **5**, pp. 459–470, February 1996.
23. C. Soussen and A. Mohammad-Djafari, “Approche multirésolution pour la reconstruction 3D de défaut en tomographie X,” in *Actes du 17*^{e} *colloque GRETSI*, (Vannes, France), pp. 1197–1200, September 1999.